

UC Berkeley

UC Berkeley Previously Published Works

Title

Coincident aboveground and belowground autonomous monitoring to quantify covariability in permafrost, soil, and vegetation properties in Arctic tundra

Permalink

<https://escholarship.org/uc/item/0pt5x6bq>

Journal

Journal of Geophysical Research Biogeosciences, 122(6)

ISSN

2169-8953

Authors

Dafflon, Baptiste
Oktem, Rusen
Peterson, John
[et al.](#)

Publication Date

2017-06-01

DOI

10.1002/2016jg003724

Peer reviewed

Coincident aboveground and belowground autonomous monitoring to quantify covariability in permafrost, soil, and vegetation properties in Arctic tundra

[Baptiste Dafflon](#)

[Rusen Oktem](#)

[John Peterson](#)

[Craig Ulrich](#)

[Anh Phuong Tran](#)

[Vladimir Romanovsky](#)

[Susan S. Hubbard](#)

First published: 06 May 2017

<https://doi.org/10.1002/2016JG003724>

Cited by: [2](#)

[UC-eLinks](#)

This manuscript has been authored by an author at Lawrence Berkeley National Laboratory under Contract No. DE-AC02-05CH11231 with the U.S. Department of Energy. The U.S. Government retains, and the publisher, by accepting the article for publication, acknowledges, that the U.S. Government retains a non-exclusive, paid-up, irrevocable, world-wide license to publish or reproduce the published form of this manuscript, or allow others to do so, for U.S. Government purposes.

Abstract

Coincident monitoring of the spatiotemporal distribution of and interactions between land, soil, and permafrost properties is important for advancing our understanding of ecosystem dynamics. In this study, a novel monitoring strategy was developed to quantify complex Arctic ecosystem responses to the seasonal freeze-thaw-growing season conditions. The strategy exploited autonomous measurements obtained through electrical resistivity tomography to monitor soil properties, pole-mounted optical cameras to monitor vegetation dynamics, point probes to measure soil temperature, and periodic manual measurements of thaw layer thickness, snow thickness, and soil dielectric permittivity. The spatially and temporally dense monitoring data sets revealed several insights about tundra system behavior at a site located near Barrow, AK. In the active layer, the soil electrical conductivity (a proxy for soil water content) indicated an increasing positive correlation with the green chromatic coordinate (a proxy for vegetation vigor) over the growing season, with the strongest correlation ($R = 0.89$) near the typical peak of the growing season. Soil conductivity and green chromatic coordinate also showed significant positive correlations with thaw depth, which is influenced by soil and surface properties. In the permafrost, soil electrical conductivity revealed annual variations in solute concentration and unfrozen water content, even at temperatures well below 0°C in saline permafrost. These

conditions may contribute to an acceleration of long-term thaw in Coastal permafrost regions. Demonstration of this first aboveground and belowground geophysical monitoring approach within an Arctic ecosystem illustrates its significant potential to remotely “visualize” permafrost, soil, and vegetation ecosystem codynamics in high resolution over field relevant scales.

1 Introduction

The northern circumpolar permafrost soil, which constitutes ~16% of the global soil area, is a critical and vulnerable region of our Earth that contains a vast pool of frozen carbon [*Tarnocai et al.*, [2009](#)]. With warming, microbial decomposition of organic-rich carbon within thawing permafrost may lead to a significant release of CO₂ and CH₄ to the atmosphere [e.g., *Davidson and Janssens*, [2006](#); *Schaphoff et al.*, [2013](#)]. Prediction of permafrost thaw and ecosystem feedbacks to climate is complicated by the numerous interactions that occur between soil hydrological, thermal, and biogeochemical processes [e.g., *Jorgenson et al.*, [2010](#)]; land surface processes including snow/water and energy fluxes [e.g., *Engstrom et al.*, [2005](#)]; vegetation processes [e.g., *Wookey et al.*, [2009](#)]; and hydrological and mechanical processes occurring in the permafrost [e.g., *Walvoord and Kurylyk*, [2016](#)]. Improved understanding of ecosystem dynamics requires the advanced characterization of soil, land surface, vegetation, and permafrost properties and their interactions. Development of new strategies to quantify aboveground and belowground codynamics is particularly challenging yet important, as such interactions influence both near-term greenhouse gas feedbacks to climate and longer-term permafrost thaw that affects the carbon cycle as well as infrastructure stability.

Several recent studies have documented correlations or associations between aboveground and belowground processes in the Arctic, motivating the need for improved monitoring systems that jointly monitor dynamics in various compartments, including the permafrost, active layer, land surface, and canopy. For example, *Natali et al.* [[2015](#)] performed plot-scale monitoring of a warming experiment and documented that soil thawing and drying increases loss of old carbon from the tundra ecosystem, but that the soil moisture has a strong control on the magnitude of the carbon release. In the Alaskan Arctic Coastal Plain, *Gamon et al.* [[2013](#)] found that vegetation productivity was strongly associated with precipitation and soil moisture, and, secondarily, with growing degree days. *Zona et al.* [[2011](#)] showed that Arctic tundra soil thermal and hydrological properties were influenced by microtopography and significantly controlled ecosystem respiration. *Wainwright et al.* [[2015](#)] documented the covariability between microtopography, soil properties, and carbon fluxes over meter to hundreds of meter length scales. Outside the Arctic environment, links between soil properties and vegetation index have been observed, such as between bulk electrical conductivity and leaf area index [*Rudolph et al.*, [2015](#)] and between

soil organic matter and spectral reflectance [Knadel *et al.*, 2011]. However, very few studies—within or outside of the Arctic—have evaluated natural variations in soil and vegetation properties with high spatial and temporal resolution, their covariability, or their interactions as a function of landscape geomorphology [e.g., Goswami *et al.*, 2011].

In particular, several studies have documented the influence of soil water content spatial and temporal variability on various processes, including thaw layer thickness and thermal properties [Romanovsky and Osterkamp, 2000], CO₂ and CH₄ emissions [Natali *et al.*, 2015], partitioning of incoming radiation into latent, sensible, and ground heat fluxes [Hinzman and Kane, 1992], photosynthesis rates [McGuire *et al.*, 2000; Zona *et al.*, 2011], and vegetation distributions and productivity. Even at temperatures below 0°C, remaining unfrozen water content is of particular interest for understanding ecosystem dynamics, because microbial activity and biogeochemical processes can still occur [Harrysson Drotz *et al.*, 2010]. A challenge is that the unfrozen water content depends on many factors, including the soil temperature as well as multidimensional relationships that consider fluid salinity and soil characteristics. Understanding if and to what extent permafrost systems experience dynamics thus requires approaches for monitoring key properties associated with these multidimensional relationships and that can integrate different required measurements. Similarly, while water content is considered a key control on vegetation dynamics, knowledge of water content alone may not be sufficient, due to the significant spatial variability in other soil characteristics that also exert an influence, such as soil and root structure and organic matter content. Thus, there is a particular need to develop new approaches that can jointly monitor and investigate soil and vegetation properties and their interactions—ideally in high resolution and in a minimally invasive manner—for improving our predictive understanding of soil-vegetation-atmosphere coupled processes.

Arctic soil characterization efforts have relied primarily on soil sample retrieval followed by laboratory analyses. Examples include the characterization of soil organic matter content [Bockheim, 2007], ice content [Kanevskiy *et al.*, 2013], and soil geochemical properties [e.g., Meyer *et al.*, 2010; Newman *et al.*, 2015]. Although such point-scale data sets provide valuable information, they are laborious to collect and process and are thus typically spatially sparse. More importantly, because acquiring soil samples is invasive and destructive, soil sampling approaches cannot be used to monitor soil processes at the same location.

Geophysical techniques have proven to be useful for both Arctic soil characterization and monitoring, providing spatially and temporally denser information than soil samples in a minimally invasive manner. Examples include the use of thermistors and dielectric permittivity sensors to obtain depth resolved profiles of temperature and soil moisture [e.g., Romanovsky and

Osterkamp, [2000](#)], ground penetrating radar to characterize thaw depth and soil moisture [e.g., Fortier et al., [2008](#); Westermann et al., [2010](#); Hubbard et al., [2013](#)], electrical resistivity tomography (ERT) to characterize soil moisture [e.g., Hubbard et al., [2013](#)], and ERT to characterize subsurface solute concentration and ice content [e.g., Dafflon et al., [2016](#)]. While ERT have shown promise for monitoring processes in permafrost environment [e.g., Hauck, [2002](#)], the use of autonomous acquisition of such time lapse data has been rarely performed in Arctic environment [e.g., Doetsch et al., [2015](#)]. To our knowledge, autonomous ERT data have never been used to explore dynamic processes in Arctic tundra permafrost environment.

Ground-based approaches to characterize and/or monitor vegetation properties typically include the use of field-portable spectrometers to acquire leaf and canopy reflectance measurements [e.g., Singh et al., [2015](#)]. These approaches generally acquire irradiance (from the sky) and radiance (from the ground) to calculate the reflectance spectrum. With this method, choices about the spectrum range and band resolution can substantially increase measurement cost. A less expensive approach is to collect only information over specific bands and calculate a spectral vegetation index using multispectral sensors or cameras. Multispectral-based vegetation indices, which minimize the effects of different sensor view angles and illumination conditions, are sensitive to changes in vegetation biophysical quantities including plant vigor and density. One of the most widely used spectral vegetation indices is the normalized difference vegetation index (NDVI), which provides a single-valued representation of the vegetation amount or vigor within a pixel [Laidler et al., [2008](#)]. The NDVI index has been used together with ground-based sampling to estimate other vegetation properties, including vegetation distribution and density [Stow et al., [2004](#)]. Several low-altitude observational studies have used green chromatic coordinate to quantify canopy greenness. The green chromatic coordinate was found to be correlated with a number of important vegetation parameters including: canopy photosynthesis in grasslands [Migliavacca et al., [2011](#)], duration of the photosynthetically active period, and gross primary productivity (GPP) inferred in various plant functional types, including deciduous broadleaf forest and grassland/crops using net ecosystem exchange measurements [Toomey et al., [2015](#)]. Spectral indices offer significant promise for vegetation characterization and monitoring, given the low cost of some of the sensors and the flexibility to acquire data at high temporal frequency and fine spatial scale using unmanned aerial system (UAS)-based platform. UAS-based surveys have been used to investigate plant distribution or infer spectral indices in various environments [e.g., Bryson et al., [2013](#)] including the Arctic tundra [e.g., Healey et al., [2014](#); Fraser et al., [2016](#)]. To the best of our knowledge, no study has evaluated relationships between such products and the subsurface properties.

The overall goal of this study is to advance coincident and continuous monitoring and understanding of aboveground and belowground interactions associated with episodic and seasonal dynamics (such as freeze-thaw) at resolutions and spatial extents relevant to ice wedge polygon heterogeneity in an Arctic tundra. To our knowledge, this is the first time that such an aboveground and belowground monitoring strategy is deployed. This novel continuous monitoring approach is expected to be very useful for quantifying ecosystem function, including characterizing initial conditions as well as the onset, duration, and spatial variability of interactions between aboveground and belowground processes that influence microbial activity and water-heat-gas fluxes.

Specific objectives of this study are to (1) develop a strategy for coincident aboveground and belowground monitoring, (2) test the approach along ice wedge polygon transects that exhibit a range of geomorphic variability, (3) investigate how unfrozen water content and salinity in soil and permafrost respond to freeze-thaw dynamics, (4) use spatially and temporally dense data (from daily to monthly sampling) to examine covariability between soil properties (including soil conductivity, soil permittivity, and thaw layer thickness), vegetation vigor (including green chromatic index and NDVI) and geomorphology, and (5) evaluate if in situ interactions and relationships between soil and landscape properties, extracted from the intensive study transect, can be extended to larger spatial extents using a UAS-based platform.

The rest of this paper is organized as follows. Section [2](#) describes the study site near Barrow, AK, which is associated with the U.S. Department of Energy (DOE) Next-Generation Ecosystem Experiment (NGEE-Arctic). The autonomous monitoring system and components are described in section [3](#), including ERT, red-green-blue (RGB), and near-infrared (NIR) sensitive cameras, and soil temperature sensors. Results and conclusions are given in sections [4](#) and [5](#), respectively.

2 Site Description and Study Transects

We performed our study at the Barrow Environmental Observatory located within the Arctic coastal region, about 6 km from the ocean shore and the village of Barrow, AK. Mean annual air temperature at the Barrow site is -11.3°C and mean annual precipitation is 173 mm [*Liljedahl et al.*, [2011](#)]. Snowmelt usually occurs in late May or early June and implies a rapid surface water runoff when ground is still frozen. The growing season starts with progressive thickening of the thaw layer and vegetation growth until about end of September, when the air temperature tends to drop below zero, where it remains until following year snowmelt. Here we define the start of the growing season as the time when the ground is entirely snow free.

The geomorphology of the Barrow coastal region is characterized by lakes, ponds, drained lake basins, and polygonal ice wedge geomorphology [Brown *et al.*, 1980; Meyer *et al.*, 2010]. The region exhibits low topographic relief, varying between about 2 and 6 m elevation, and is dominated by different types of polygons, including low-centered polygon (LCP), flat-centered polygon (FCP), and high-centered polygon (HCP) [e.g., Mackay, 2000; Hinkel *et al.*, 2001; Hubbard *et al.*, 2013]. These different types of polygons, which represent various stages of ice wedge development and degradation, govern local microtopography. The polygon-based microtopography in turn influences snow thickness [Wainwright *et al.*, 2015], thaw layer thickness [e.g., Gangodagamage *et al.*, 2014], and drainage and thus soil moisture at the site [e.g., Hubbard *et al.*, 2013; Engstrom *et al.*, 2005]. Polygon-driven water distribution can influence a cascade of biogeochemical processes, including both aboveground vegetation responses and belowground microbially mediated processes [e.g., Hubbard *et al.*, 2013; Zulueta *et al.*, 2011]. For example, Wainwright *et al.* [2015] demonstrated that polygon type is significantly correlated with CO₂ and CH₄ fluxes at the study site.

Vegetation in the coastal tundra near Barrow, AK, generally consists of moss, lichen, dwarf shrubs, forbs, and graminoids such as *Carex aquatilis* [e.g., Villarreal *et al.*, 2012]. In a study located very close to our study site, Zona *et al.* [2011] has shown that the wet troughs and centers of LCPs and FCPs are primarily filled by *Carex aquatilis* and by mosses (*Sphagnum* spp.). In the relatively dry areas, such as the rims of LCPs and the centers of HCPs and some FCPs, mosses (*Sphagnum* spp.) and lichens dominate. On dry polygon rims, standing dead-plant materials cover up to 60%, with limited presence of leaf litter and peat. In intermediate and low-center areas, standing dead-plant materials, leaf litter, and peat are present in almost the same amount and altogether cover about 50% of the ground surface [Zona *et al.*, 2011].

The soil active layer thickness associated with ice wedge polygonal regions near Barrow, AK, varies spatially between 25 to 65 cm [e.g., Hinkel and Nelson, 2003; Shiklomanov *et al.*, 2010]. The thickness of the seasonally thawed layer is influenced by several factors, including vegetation, snow insulation, soil physical properties, water content, and seasonal temperature variations [Hubbard *et al.*, 2013]. Several studies, including Mackay [2000] and Hubbard *et al.* [2013], documented relationships between geomorphic features (such as different types of polygons) and soil properties (such as ice content, organic content, temperature, and soil type). Wainwright *et al.* [2015] showed that the soil moisture content and thaw layer thickness vary distinctly under HCP, FCP, and LCP, and that the driest conditions and smallest thaw layer thickness are generally associated with the centers of HCPs and topographic highs.

Permafrost is conventionally defined as material having a temperature at or below 0°C for two or more years [Washburn, 1979]. The permafrost at the study site includes frozen soil, ice wedges, ground ice, and saline permafrost, with striking lateral and vertical variability [e.g., Leffingwell, 1915; Dafflon et al., 2016]. The ice content in the upper permafrost around Barrow, AK, is high at shallow depths and decreases with depth [Sellmann et al., 1975; Brown et al., 1980, Kanevskiy et al., 2013]; analysis of soil cores collected at this site reveals ice content as high as 75% in the top 1 m of permafrost and ice content as low as 40% at 2.5 m depth. This decrease in porosity with depth varies spatially and tends to be most significant when the permafrost salinity also increases with depth [Dafflon et al., 2016]. Partially unfrozen saline permafrost has been found at variable depths beneath frozen permafrost layers around Barrow, AK [e.g., O'Sullivan, 1966; Brown, 1969; Williams, 1970; Yoshikawa et al., 2004]. Site core samples at 3–6 m depth [O'Sullivan, 1966; Brown, 1969; Sellmann et al., 1975] have shown salinity values up to 2 times seawater salinity [O'Sullivan, 1966]. Bulk electrical resistivity imaging, seismic, and analysis of core samples at the study site [Dou and Ajo-Franklin, 2014; Dafflon et al., 2016] suggested that the partially unfrozen saline permafrost is spatially extensive and heterogeneous.

We developed nested observational transects within the study site to test a new strategy for jointly monitoring permafrost, soil, and vegetation dynamics and their interactions (Figure 1). The observational layout consisted of a 35 m intensive transect, which traversed HCP, FCP, and LCP geomorphic features. At the site, the HCP has a topographic high in his center, with no ridge between the center and the trough. The FCP has a center that is topographically slightly lower than the surrounding ridge. While a LCP typically has a center that is substantially lower than the surrounding ridge, the ridge of the LCP shown in Figure 1 is pronounced on one side but smaller on the side that we traverse. We still refer to it as a LCP due to the pronounced ridge on one side and because the polygon is much larger than the nearby FCP and HCP, which is typical for LCPs in this site [Wainwright et al., 2015]. The HCP, FCP and LCP defined here are associated with variations in vegetation and geomorphology described by previous studies near or at this site [Hubbard et al., 2013; Wainwright et al., 2015].

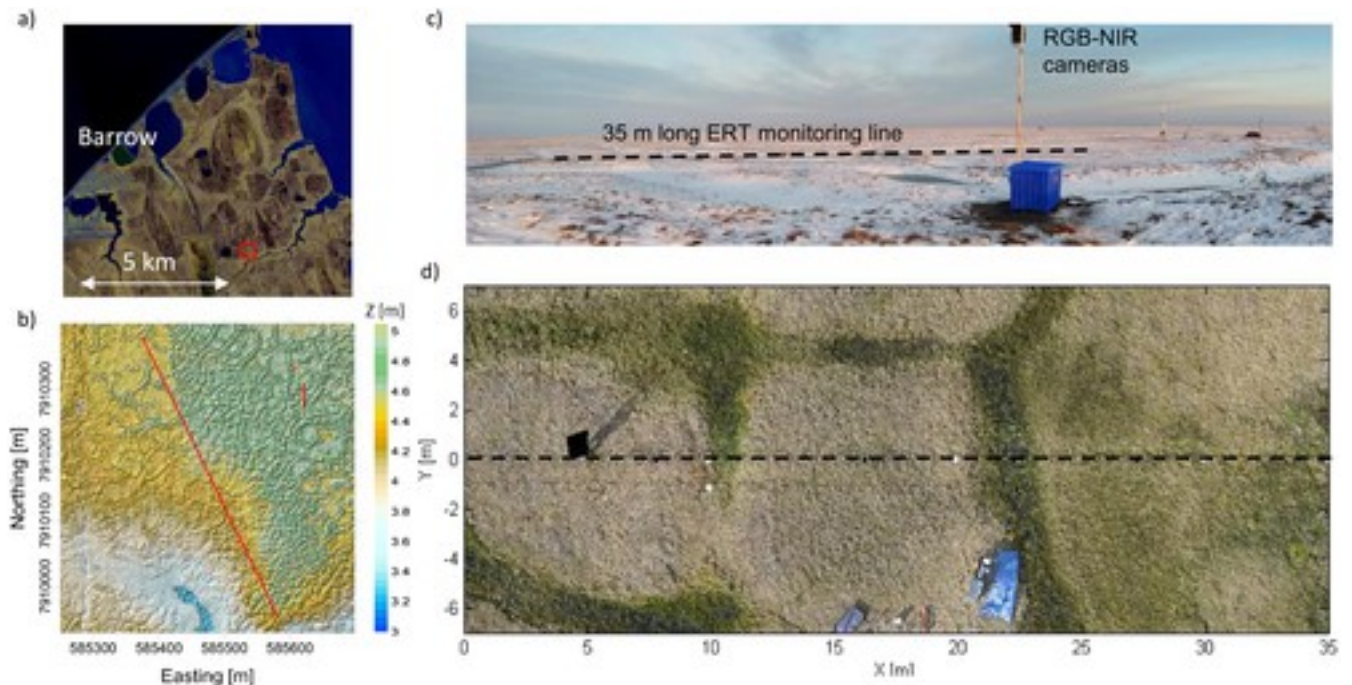


Figure 1

[Open in figure viewer](#) [PowerPoint](#)

(a) Location of the study site near Barrow, Alaska, U.S. (b) Shaded topographic map of the investigated site showing the location of the 35 m long transect where measurements were acquired at least daily (small red line) and a 475 m long transect (long red line), where measurements were acquired occasionally. (c) View of the 35 m long monitoring transect with the ERT line (dash line) and pole-mounted cameras, the latter located 18 m from the ERT line and having the whole line in their field of view. (d) Aerial view of the ERT transect (dashed line), which traverses different types of polygons. Temperature was monitored at depths of 0.03, 0.5, 1, and 1.5 m belowground surface and at lateral distances of 7.5, 22 and 27 m along the transect.

[Caption](#)

A wide variety of aboveground and belowground autonomous sensors were installed along the intensive transect (Figure 1), which collected daily or more frequently measurements for a full year. Approximately parallel to but offset from the intensive transect, was a 475 m “regional” transect, where measurements were collected manually as part of a previous study [Hubbard *et al.*, 2013]. As will be described in section 3, the intensive transect was used to develop coincident monitoring strategies and understanding of aboveground and belowground interactions, whereas the regional transect (Figure 1b) was used to test the ability to scale the strategy up to larger areas, as needed for improving our understanding of ecosystem feedbacks to climate.

3 Methods: Background and Data Sets

3.1 Electrical Conductivity Imaging of Permafrost and Soil Systems

3.1.1 ERT Method and Petrophysical Relationships

ERT data are collected using electrodes inserted in the ground, where the current is injected between two electrodes and the electrical potential difference is measured between two others. With this method, numerous measurements are acquired using different combinations of electrodes along the transect. The acquired resistance data are then inverted to estimate the spatial distribution of soil electrical resistivity (or its inverse, the electrical conductivity) [e.g., [Kemna, 2000](#)]. The electrical conductivity (or resistivity) response is influenced by subsurface properties such as water/ice content, fluid electrical conductivity, lithological properties such as clay content, and soil temperature [e.g., [Archie, 1945](#); [Revil et al., 1998](#); [Friedman, 2005](#)]. Due to the sensitivity of electrical conductivity to various subsurface properties, ERT has been widely used to investigate the spatial and temporal changes of soil, vadose zone, aquifer, and increasingly in permafrost systems [e.g., [Hauck, 2002](#); [Krautblatter et al., 2010](#); [Yoshikawa et al., 2006](#); [Hubbard et al., 2013](#)]. In Arctic environments, ERT has been used successfully to characterize a range of properties. Examples include the spatial distribution of various lithological units [e.g., [Yoshikawa et al., 2004](#); [Overduin et al., 2012](#)], active layer properties such as thickness and water content [[Hubbard et al., 2013](#)], and permafrost properties such as bulk resistivity, ice content, and salinity [e.g., [Fortier et al., 2008](#); [Dafflon et al., 2013](#)]. ERT data have also been used to constrain thermal simulation [[McClymont et al., 2013](#)] and to investigate the dynamics of freeze-thaw processes and water-to-ice transitions [[Overduin et al., 2012](#); [Wu et al., 2013](#)]. Autonomous acquisition of ERT time lapse data has been used to monitor freeze-thaw dynamics in alpine permafrost environments [e.g., [Hauck, 2002](#)] and in seasonally frozen Arctic environments [e.g., [Doetsch et al., 2015](#)]. To our knowledge, this study is the first to explore the use of autonomous acquisition of ERT time lapse data to monitor seasonal changes in an Arctic continuous permafrost environment and the first to couple such measurements with aboveground measurements.

Petrophysical relationships are required to understand and extract useful information about subsurface properties from ERT data. The relationship at a given temperature T between the bulk electrical conductivity σ_b [S/m], the fluid conductivity σ_f [S/m], the porosity ϕ [m³/m³], and the fractional (unfrozen) water saturation S_w [m³/m³] can be expressed based on Archie's law [[Archie, 1945](#)] by

$$\sigma_b = S_w^n \phi^m \sigma_f \quad (1)$$

where n and m are defined as the Archie saturation and cementation exponents, respectively. While a surface conduction term can be added on the right side of the equation [e.g., [Revil, 2012](#)], here we assume surface conduction is negligible and thus do not include it. The unfrozen water content W is equal to $S_w \times \phi$, while we decided to keep the porosity constant over time. The m and n exponents in [1](#) vary as a function of pore geometry; they are often assumed equal to a value between 1.5 and 1.8 for unconsolidated sediments [e.g., [Sen et al., 1981](#)]. For this study, given that the saturation and cementation exponents likely increase with soil freezing, we set both exponents equal to 1.8.

The fluid conductivity at a specific temperature is defined as

$$\sigma_f = [1 + 0.019(T - 25)]F_c \sum_i \beta_{i25} |z_i| M_i \cong [1 + 0.019(T - 25)]C/k_e(2)$$

F_c is Faraday's constant (Cmol^{-1}) and M_i , β_i , and z_i are the concentration (mol/m^3), ionic mobility ($\text{m}^2 \text{V}^{-1} \text{S}^{-1}$), and valence of the i th species, respectively [[Revil, 2012](#)]. The summation in [2](#) is performed over all dissolved ionic species; for this study, Na^+ and Cl^- are assumed to be the primary constituents. Temperature T influences the fluid viscosity and the mobility of ions, which both influence fluid conductivity. Here we use a slope of 0.019, which translates to a 1.9% change in fluid electrical conductivity per degree Celsius [[Hayley et al., 2007](#)]. When information on the dissolved ionic species is not available, a simplified approach is to link fluid conductivity (S/m) at 25°C to the total dissolved solid (TDS) concentration C (g/L) with k_e being a correlation factor commonly set equal to 6.4 for groundwater [e.g., [Atekwana et al., 2004](#)]. [Dafflon et al. \[2016\]](#) used a k_e equal to 7.1 based on our analysis of saline permafrost soil cores (not shown).

Special consideration is needed to estimate the subsurface unsaturated water content from the bulk electrical conductivity signature when the temperature drops below the freezing point. In this case, the bulk conductivity decreases until all the water is frozen. In the presence of freshwater, the use of a logarithmic relationship to relate decrease in bulk conductivity with decrease in water content and temperature [[McGinnis et al., 1973](#)] has shown satisfactory results for loose soils [e.g., [Hauck, 2002](#); [Wu et al., 2013](#)]. In general, pure ice is formed during freezing and solutes are rejected into the unfrozen solute [e.g., [Hivon and Segó, 1995](#); [Marion, 1995](#)]. A simple and commonly used conceptual model is that the increase in the in situ solute concentration is proportional to the decrease in the unfrozen water due to salt exclusion during ice formation [[Hivon and Segó, 1995](#); [Minsley et al., 2015](#); [Dafflon et al., 2016](#)]. [Minsley et al. \[2015\]](#) added an exponent to the saturation term to account for variable loss of solute from the pore space due to diffusion or other transport processes, so the equation is given by

$$C = C_0 S_w^{-a} = C_0 \left(\frac{W_0}{W} \right)^a, \quad (3)$$

where C_0 is the initial solute concentration (referred as solute concentration in fluid extracted of a core sample after being thawed) and W_0 is the total water content. Setting the exponent a equal to 1 assumes that increase in in situ solute concentration fully balances the decrease in the unfrozen water content W [Dafflon et al., 2016]. Setting a to 0.8 implies variable loss of solute from the pore space [Minsley et al., 2015], and setting it to 0 means no change in solute concentration in the remaining unfrozen water content during freezing. Assuming that the exponent a is close to 1 means that a soil at a given temperature, with specific unfrozen water content and in situ solute concentration, can correspond to various soil that have equal product of initial solute concentration and total water content. While equation 3 can be used with equations 1 and 2 to predict unfrozen water content from electrical conductivity given that the initial concentration, total water content, and exponents a and n are reasonably known or estimated, another alternative is to assume that the solute concentration is at the equilibrium at each temperature [Hivon and Sego, 1993] and can be estimated using a sodium chloride water binary phase diagram [e.g., Maidment, 1993, Potter et al., 1978; Velli and Grishin, 1983; Hall et al., 1988; Bodnar, 1993]. The equation of Potter et al. [1978] for sodium chloride, very similar to Bodnar [1993], is defined as

$$C = MM_{\text{NaCl}} * (0.30604 dT - 2.8598e-3 dT^2 + 4.869e-6 dT^3)_{(4)}$$

where dT is the freezing point depression (i.e., the modulus of the temperature at which a solute starts freezing) and MM_{NaCl} is the molar mass of NaCl (58.44 g/mol). This approach assumes that the freezing behavior of the water in soil is very similar to the freezing behavior of water only. The above equations have been used at the NGEE-Arctic field site to estimate total soil water content and initial solute concentration as well as in situ unfrozen water content from ERT data [Dafflon et al., 2016]. In particular, the total water content and initial solute concentration were estimated using a linear relationship observed between total water content and initial solute concentration (extracted from collocated core samples), the relationships expressed in equations 1 to 4, and by assuming the exponent a equal to 1. Dafflon et al. [2016] also showed that due to uncertainty and simplification associated with the petrophysical relationships described above, uncertainty in the estimation of total water content, initial solute concentration, and in situ unfrozen water content were each on the order of 20–30%.

3.1.2 ERT Acquisition and Inversion

We acquired ERT data along the intensive transect daily between August 2013 and September 2014 using a MPT-DAS-1 system with a 0.5 m electrode spacing. Data acquisition, quality control, acquisition parameter update, and data transfer were performed autonomously using a remote computer. The data were acquired in the frequency domain using various geometries, including dipole-dipole and Wenner-Schlumberger configurations; both resistance and phase shift data were recorded. Here we focus on data collected using the Wenner-Schlumberger configuration, because data quality is higher with this configuration, especially during the freezing season.

All the data were inverted for electrical resistivity using CRTomo, which utilizes a smoothness-constrained approach based on a finite-element algorithm and solves for resistivity within a two-

dimensional region of interest [Kemna, [2000](#)]. The electrode locations and elevations were adjusted based on Real Time Kinematic (RTK) GPS measurements. Low-quality measurements were removed prior to the inversion, including signals associated with measured potentials less than 1 mV. Reciprocal measurements acquired during the growing season were used to select data with error repeatedly smaller than 2% between reciprocal and normal measurements. The inverted data sets contained generally about 680 measurements, with a minimum number of ~600 from mid-December to mid-May, during which the contact resistances deteriorate. Data assessment and selection during this period was more challenging, and thus, associated regularization constraints were set to obtain relatively smooth models. The inversion of each data set was done with the same parameterization, independently but with the first time lapse inversion used as the prior model. An anisotropic ratio of two between horizontal and vertical regularization was used. We utilize the increase in relative mean absolute difference (mad) between measured and simulated logarithms of apparent resistivity as a partial indicator of noise increase in the data.

ERT data were also manually acquired in September 2012 along a 472 m long transect with 0.5 m electrode spacing and a roll-along strategy. Data were acquired using a dipole-dipole configuration. Along the regional transect, the largest distance between the closest injection and potential electrode was 18 m, while largest distance between the two injection (or potential) electrodes was 3 m. Processing and inversion have been performed similarly as described above; the reader is referred to *Hubbard et al.* [[2013](#)] for more details on the regional-scale transect.

3.2 Landscape Imaging and Vegetation Index Mapping

3.2.1 Multispectral Imaging of Land Surface and Vegetation

Ground-based monitoring of vegetation density and vigor using reflectance properties can be performed using a variety of acquisition platforms (including hand held, pole based, and cart mounted) and sensors (including spectrometer and multispectral). These ground-based measurements permit acquisition of measurements at spatiotemporal resolutions not achievable from satellite observations. Ground-based dual-detector field portable spectrometers have been used to monitor leaf and canopy reflectance at various spatial resolutions, up to the leaf scale [e.g., *Gamon et al.*, [2013](#)]. Dual-detector field portable spectrometers acquire with very high band resolution radiance (radiation from the ground surface) and irradiance (radiation from the sky) data simultaneously, thereby permitting reliable surface reflectance measurement under varying atmospheric conditions [e.g., *Goswami et al.*, [2011](#); *Gamon et al.*, [2013](#); *Singh et al.*, [2015](#)]. Low cost multispectral sensors offer much lower band resolution and only partial

coverage of the energy spectrum compared to spectrometers; they are primarily used to calculate indices such as NDVI or green chromatic coordinate. Such indices have been inferred from spectrometers, as well as from multispectral sensors, three-band standard RGB cameras, and/or standard cameras modified to sense near-infrared band [e.g., *Sonnentag et al.*, [2012](#); *Nijland et al.*, [2014](#)].

While vegetation indices can be obtained using both standard and modified cameras, documentation of the relative benefits or limitation of the different approaches is still limited. Consumer cameras are designed for taking pictures in a manner that resemble the human vision. This approach leads to considerable overlap between red and green sensitivity and little to no NIR specific sensitivity (the right channel may be slightly sensitive to NIR). Although standard cameras can be converted to sense NIR, *Nijland et al.* [[2014](#)] showed that converted cameras performed worse than standard color cameras in a monitoring setting, which supports the use of standard color cameras as simple and affordable tools for the monitoring of plant stress and phenology. Indeed, many ground-based surveys and long-term efforts have monitored phenology using standard color cameras and green chromatic indices, green chromatic excess index, or green chromatic coordinate [e.g., *Woebbecke et al.*, [1995](#); *Richardson et al.*, [2007](#); *Migliavacca et al.*, [2011](#); *Sonnentag et al.*, [2012](#)]. Such color indices derived from digital repeat photography have provided information about the phenology of diverse plant communities and functional types [e.g., *Richardson et al.*, [2007](#)]. *Migliavacca et al.* [[2011](#)] has documented the correlation between green chromatic coordinate and canopy photosynthesis in grasslands, and *Toomey et al.* [[2015](#)] has documented the correlation between green chromatic coordinate and the duration of the photosynthetically active period, as well as the gross primary productivity (GPP), inferred in various plant functional types including deciduous broadleaf forest and grassland/crops using net ecosystem exchange measurements.

In summary, standard cameras (or multispectral cameras with limited number of bands) primarily provide vegetation indices and do not provide absolute values of reflectance. However, their low-cost and high spatial resolution make them attractive for mounting on a pole and/or on UAS platforms. Recent development of UAS platforms and structure-from-motion-based reconstruction techniques—also referred as PhoDAR—enables simple reconstruction of georeferenced mosaic and digital surface model [e.g., *James and Robson*, [2012](#); *Fonstad et al.*, [2013](#)], and thus straightforward inference of vegetation indices from multispectral cameras.

For this study, we built upon the previous studies to develop our aboveground monitoring strategy. In particular, we used standard cameras mounted on a pole to acquire data with high

temporal resolution along an intensive transect, while using a UAS-based platform to acquire data along a regional transect but at a single point in time.

3.2.2 Aboveground Data Acquisition and Processing

We estimated vegetation indices along the intensive transect at the study site using two standard digital single-lens reflex (DSLR) cameras mounted on a pole, which were located approximately 3 m above the ground and approximately 17 m away from the ERT line. The Canon EOS Rebel SL1 cameras featured a APS-C CMOS sensor, 18 Mpix resolution, and a CANON EF 10–22 mm lens set at 90° field of view. The internal near-infrared cut filter was removed from one of the cameras and replaced with a high-pass color filter (that allowed transmission of wavelengths above 720 nm) to enable imaging in near-infrared wavelengths. The cameras were operated a few times per week from 8 May to 25 June and then fully operated from 28 June to 11 August 2014, capturing four successive image frames every 4 h at very high quality JPEG format and 5184 × 3456 pixel resolution. With this resolution, the interval between each couple of electrodes (0.5 m spacing) is covered by about 70 pixels, leading to a resolution of about 1 cm. The cameras were controlled with a commercial software installed on a small computer that enabled remote data acquisition and data transfer. Acquisition ceased on 11 August due to the failure of a USB cable, which could not be replaced before the end of the summer season.

Since the fields of view of RGB and NIR images did not overlap exactly, a transformation to register RGB and NIR images correctly was performed using 80 control points—including eight target corners and 72 markers on electrical cable. Control points were automatically detected in the images and a nonlinear optimization of Levenberg-Marquardt method was used for the transformation. Images from two highly degraded rainy and foggy day were discarded from the set. The obtained NDVI and green chromatic indices for each sampling location were averaged over the images of the same day, for the period of 1 July to 11 August. Sampling locations were identified by taking an 10 × 10 cm window located next to each electrode and in midway between two consecutive electrodes and computing the block average of the NDVI defined as $(\text{NIR} - \text{R})/(\text{NIR} + \text{R})$ and green chromatic coordinate defined as $(\text{G}/(\text{R} + \text{G} + \text{B}))$, where B, G, R and NIR represent the blue, green, red, and near-infrared channel, respectively. Images were corrected for various light conditions by considering color plane intensities of a pair of points on eight ground control targets along the ERT line and tracking the variation of the intensities in time. A linear transform using ground control targets was found to be optimal for inferring green chromatic coordinate from RGB images, and nonlinear transform was used to infer NDVI values from RGB and NIR pictures. Results show that although both NDVI and green chromatic

coordinate captured spatial and temporal landscape variability with similar trends, the green chromatic coordinate was much less sensitive to changes in light and weather conditions.

The green chromatic coordinate was also inferred at a single point in time from a mosaic acquired using a kite-based platform located approximately 40 m above the ground. The regional transect corridor extended 500×40 m and was collected in July 2013. The pictures were acquired with a Sony Nex-5R camera featuring a APS-C size CMOS sensor, 16 Mpix resolution and a 16 mm lens. The camera was selected as a trade-off between image quality obtained from a full-frame sensor DSLR camera and a lightweight small-sensor compact digital camera. About 80 overlapping kite images were processed with a commercial software and using high-accuracy GPS-surveyed ground-control points to generate a 2D orthomosaic image and a digital surface model, with less than 5 cm uncertainty in all directions and 2 cm resolution. The reader is referred to *Dafflon et al.* [2016] for more details. Here the reconstructed mosaic was used only to infer green chromatic coordinate which is then compared to shallow electrical conductivity extracted from a collocated ERT transect to evaluate representativeness of the results obtained at the monitoring site. The inferred green chromatic coordinate map shows similar values and variability to measurements observed along the intensive transect, although they cannot be precisely compared because they were not collocated in time and space.

3.3 Point-Scale Measurements

Several types of point-scale measurements were acquired both autonomously and manually along the intensive monitoring transect at various temporal intervals. Active layer measurements were acquired with a tile probe every 0.5 m along the transect on 18 July 2013, 1 October 2013, 1 July 2014, 17 August 2014, and 21 September 2014. Snow depth measurements were acquired at the same stations November 20 2013 and April 22 2014. Time domain reflectometry (TDR) measurements were acquired on 1 October 2013 and 1 July 2014 using a soil-moisture-Trase-system TDR with two 15 cm waveguides placed 5 cm apart and pushing the probe vertically in the ground.

Soil temperature was autonomously monitored with thermistors installed at four different depths (0.03, 0.5, 1, 1.5 m) in a 2.54 cm diameter pipe at three different locations along the intensive transect (at 7.5, 22 and 27 m from the south end of the transect). Thermistors accuracy is about 0.05°C , and uncertainty in placing them is about 2 cm. A fourth temperature depth profile, located at 16.25 m, did not provide any data because it stopped working soon after its installation. Also, the thermistors initially installed at 7.5 and 22 m rose 6 cm due to heave that likely occurred in spring 2014. This primarily impacted the reliability of the sensors located at

0.03 m depth, which moved above ground surface; data from this sensor were not considered after May 2014. We also used a temperature depth profile acquired on a HCP center located about 100 m from the intensive monitoring site to evaluate soil temperature variations at 3 m depth. We used this “offset” temperature measurement because a deep measurement was not available along our intensive transect. While not ideal, the lateral variability in temperature at 3 m belowground surface is relatively small.

4 Results and Discussion

4.1 Active Layer and Permafrost Responses to Freezing

We first explore the responses of the ERT and point-scale measurements to investigate seasonal to annual freeze-thaw dynamics occurring within the top 4 m below the surface, which includes the active layer and permafrost (Figures 2-5). The spatiotemporal distribution of bulk resistivity in the ERT time lapse images between 15 August 2013 and 17 August 2014 (Figure 2) shows that freezing and thawing behavior of the active layer covaries with geomorphology. For example, the resistive (dry) center of the HCP (left side of the monitoring transect), which has an electrically resistive thaw layer during the growing season, experiences earlier freezing compared to the thaw layer beneath the other polygon types as expressed by a relatively significant increase in resistivity. In contrast, the thaw layer beneath the LCP (Figure 2, right column), which is characterized by low resistivity at the beginning of the monitoring period, reaches the same low resistivity value about 2 months later than the thaw layer beneath the HCP. Figure 3 illustrates how temperature and electrical conductivity change as a function of time, depth, and position relative to different types of polygons. This figure reveals that the trend and timing of temperature and electrical conductivity responses are similar and confirms that the earliest freeze of the thaw layer occurred in the center of the (relatively dryer) HCP, which also shows the earliest thawing at the very beginning of the growing season only. While troughs and ice wedges represent particular locations where ice and water contents as well as heat fluxes can strongly differ from other locations, ice wedges are not clearly distinguished in Figure 2. Ice wedges may not be distinguishable on this figure because they may have limited contrast with surrounding soil conductivity or may not be resolvable using the smoothed and laterally constrained ERT inversion approaches. We note that *Dafflon et al.* [2016] showed that ice wedges are clearly identified using ERT data only when the permafrost has a significantly lower ice content and higher salinity than the ice wedge.

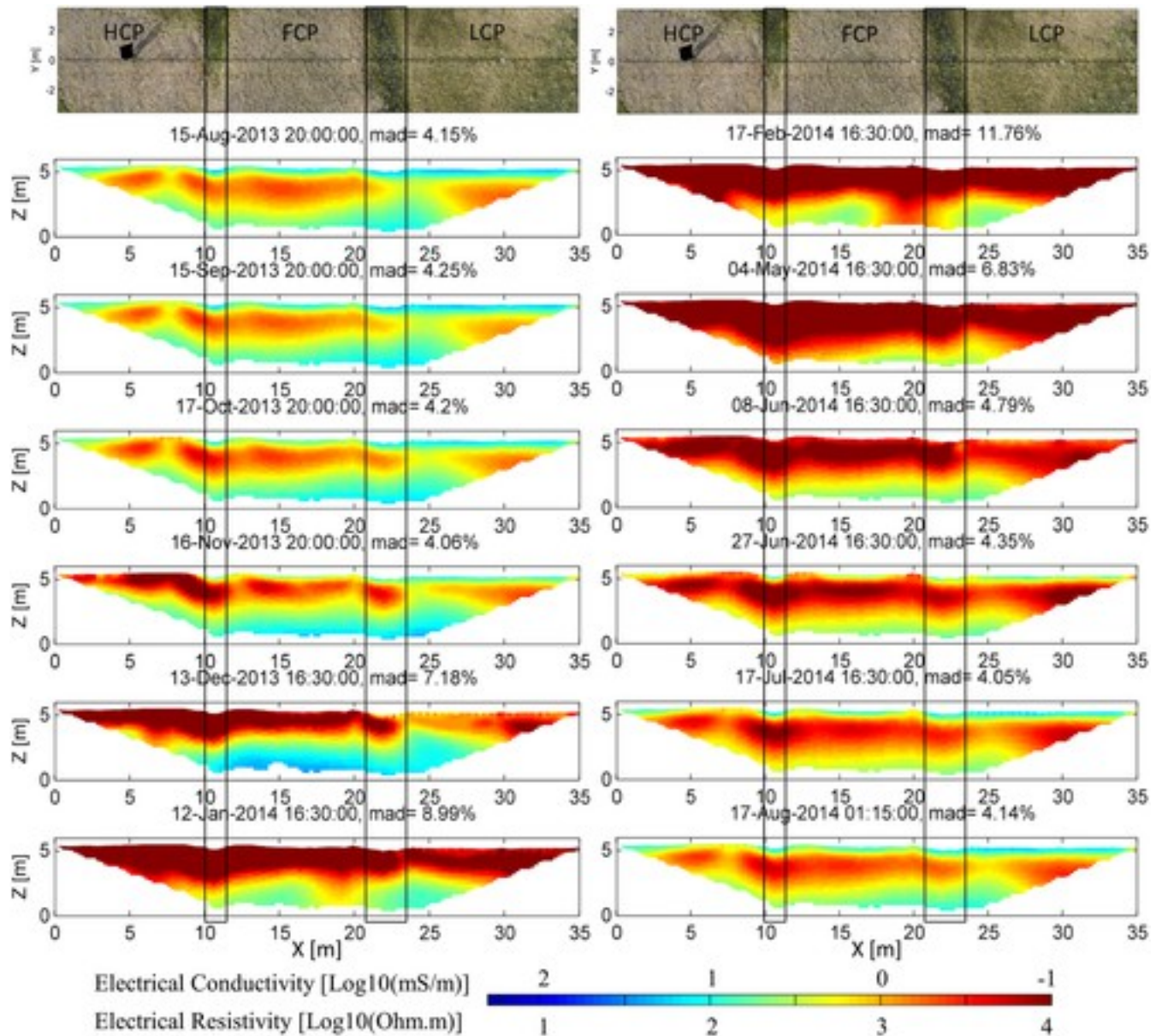


Figure 2

[Open in figure viewer](#) [PowerPoint](#)

Soil electrical resistivity (ohm m) or conductivity (mS/m) estimates (\log_{10} scale) at about 1 month intervals between 15 August 2013 and 17 August 2014. The x axis indicates the distance along the intensive transects (Figure 1d), and the z axis shows the elevation above means sea level. The relative mean absolute difference (mad) between measured and simulated logarithms of apparent resistivity is shown above each panel.

[Caption](#)

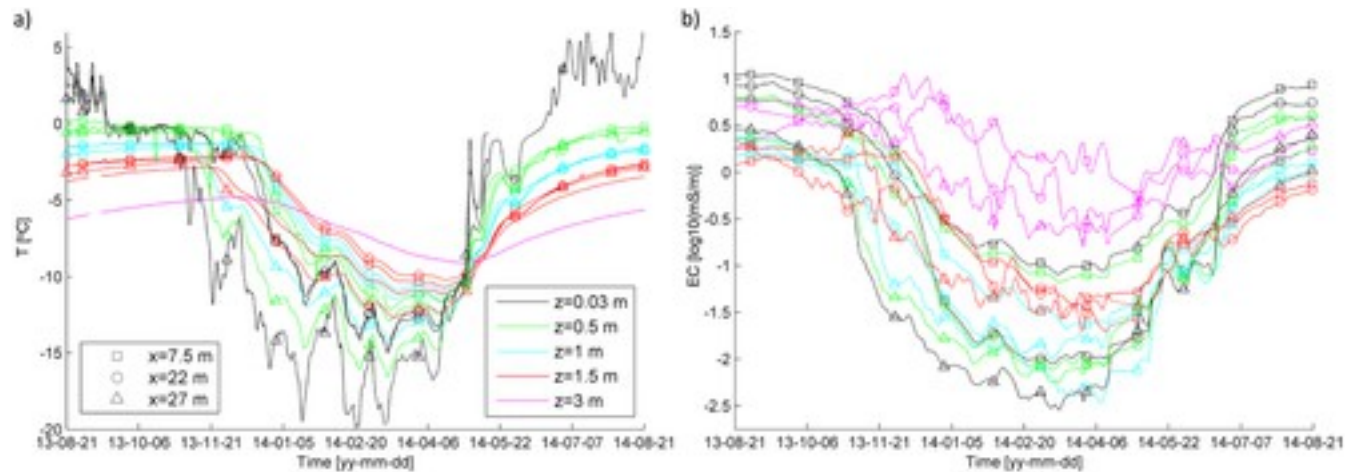


Figure 3

[Open in figure viewerPowerPoint](#)

(a) Temperatures at depths of 3 cm, 50 cm, 100 cm, and 150 cm at different locations along the intensive transect (refer to Figure 1d) including 7.5 m (HCP center), 22 m (LCP trough) and 27 m (LCP center). The temperature at 1.5 m and 3 m depths under a FCP center located 100 m away from the ERT transect is also shown. (b) Electrical conductivity values extracted from the ERT data at the same locations along the intensive monitoring transect and at all depths shown in Figure 3a using the same color coding.

[Caption](#)

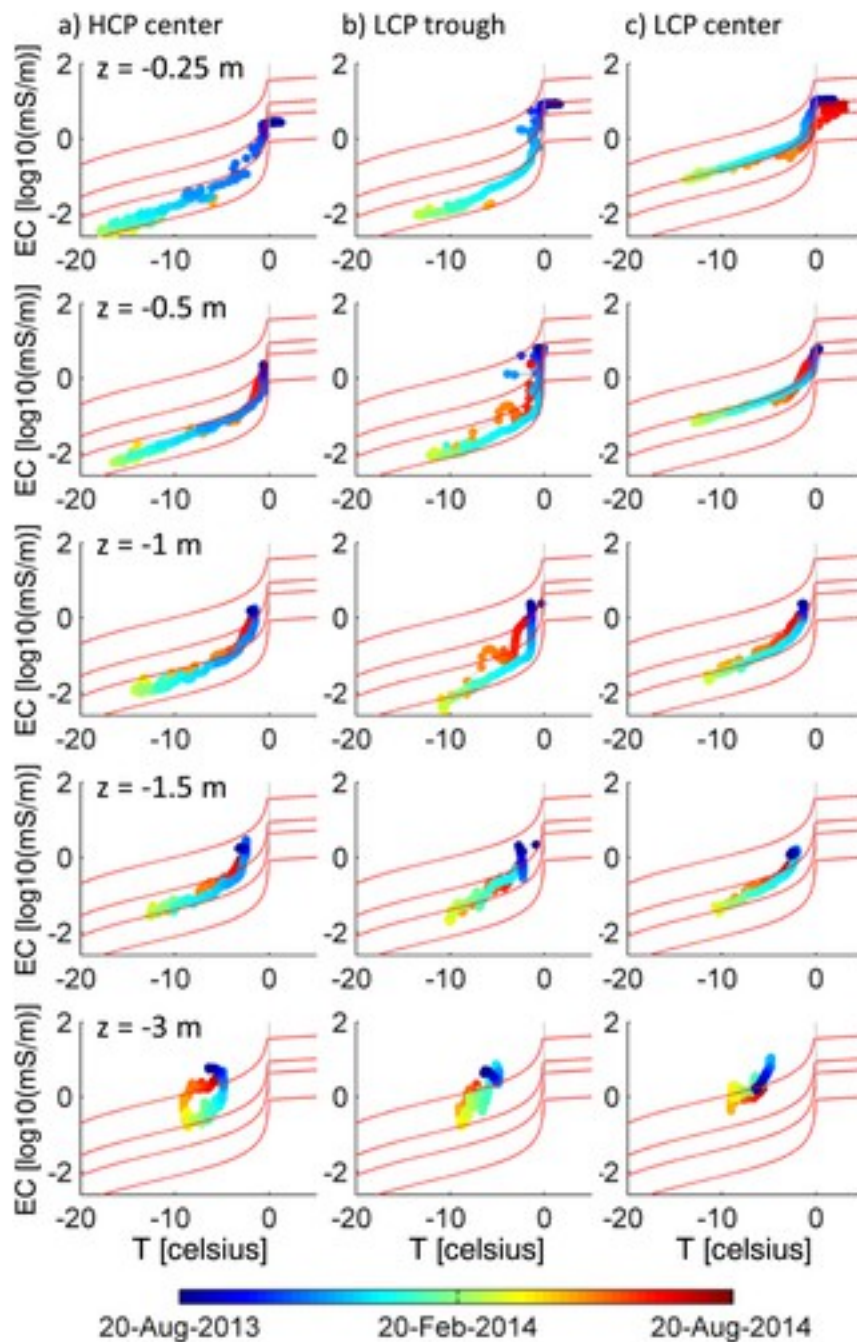


Figure 4

[Open in figure viewer](#)[PowerPoint](#)

Subsurface electrical conductivity versus temperature relationships from August 2013 to August 2014, shown as a function of depth (rows) and various locations along the transect, including at (a) 7.5 m (HCP center), (b) 22 m (LCP trough), and (c) 27 m (LCP center). The temperature-conductivity relationships shown in red permit qualitative comparison between responses at the various locations. These curves were obtained using equations 1 to 4 and were parameterized with: total water content equal to 0.4, initial solute concentration equal to 0.2, 0.5, 1, and 3 g/L (from lowest to top red line) and with exponents m and a equal to 1.8 and 1, respectively.

[Caption](#)

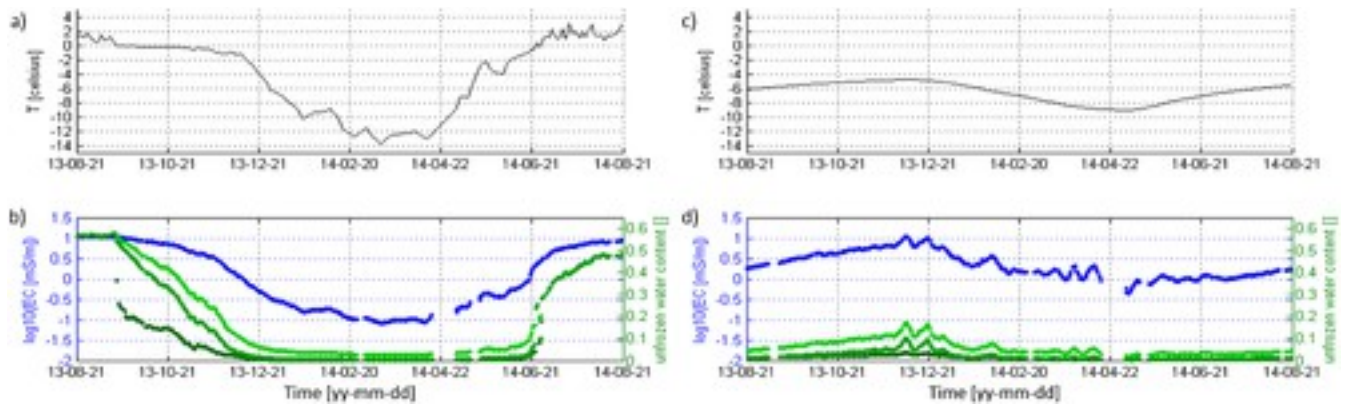


Figure 5

[Open in figure viewer](#) [PowerPoint](#)

Measurements and estimates over time at 27 m horizontal distance along the transect and at 0.25 m depth, including (a) temperature, (b) measured electrical conductivity (blue) and estimated unfrozen water content obtained using various approaches, including from electrical conductivity using equations 1, 2, and 3 with a equal to 0.5 (thick lime green line) and 1 (thick kelly green line), and from electrical conductivity and temperature using equations 1, 2 and 4 (thick dark green). Equation 3 was parameterized with an initial solute concentration of 0.4 g/L and total water content equal to 0.6. (c and d) Similar estimation as Figures 5a and 5b at 27 m horizontal distance along the transect but in the permafrost at 3 m depth, with equation 3 parameterized with initial solute concentration equal to 5 g/L and total water content equal to 0.4. In both Figures 5b and 5d exponent m was set equal to 1.8.

Caption

While permafrost is generally assumed to be completely frozen yearround and for consecutive years, Figure 2 reveals dynamics due to nonnegligible changes in water content and solute concentration in this region. For example, at about 3 m depth the electrical resistivity varies between 50 ohm m and 3000 ohm m with the lowest values in December, which corresponds to the warmest time of the year at that depth (Figure 2). This behavior is confirmed in Figure 3, where temporal variations in temperature at various locations and depths along the intensive transect are compared with collocated electrical conductivity data extracted from the ERT time lapse data. Figure 3 also shows that the temperature inflection point, which occurs at the beginning of the freezing, is consistent with the inflection point in the soil electrical conductivity response, and that the seasonal freezing of unfrozen water in the saline permafrost and in the active layer have different timing due to the heat transfer. Changes in unfrozen water content and solute concentration drive the changes in electrical conductivity much more than the temperature effect on fluid conductivity. Also, the conductivity increases that occur when the temperature increases (and vice versa) suggest that the related increase in unfrozen water content has a greater influence on the bulk electrical conductivity than the decrease in solute concentration. This is consistent with the fact that the unfrozen water saturation varies to the power of the exponent n (which is larger than 1) in Archie's law, and that the exponent a is likely smaller than

1. Finally, while the lateral variability in the saline permafrost and its link with geomorphological features cannot be clearly identified along the intensive monitoring site, *Dafflon et al.* [2016] showed that at larger scale, the saline permafrost tends to be more shallow in HCP regions, which is where surface water drainage efficiency is relatively higher.

Crossplots between in situ temperature and electrical conductivity, overlying various models of electrical conductivity freeze-up curves calculated from equations 1 to 4, allow us to explore the variability in freeze-thaw processes at different depths and locations along the intensive transect (Figure 4) and to compare electrical conductivity responses at various depth but at the same temperature. The temperature-conductivity relationships show relatively similar trends, including a strong decrease in conductivity close to the freezing point and then an asymptotic behavior at lower temperature. However, the absolute values are very different. The temperature-conductivity relationships at 3 m depth reveals that the initial solute concentration at this depth is significantly higher than at shallower depth and can produce the observed high electrical conductivity values even when the temperature is well below 0°C. This occurs even though the total water content is smaller at 3 m depth than at ~0.75 m depth. These findings are consistent with those of *Dafflon et al.* [2016], who showed that the porosity is on the order of 70% in the shallow permafrost and decreases to 40% at about 3 m depth due to limited ice segregation in zones with high fluid salinity. In addition, the temperature-conductivity crossplot at 0.25 m depth in LCP center (Figure 4) shows that the larger conductivity values (due to higher water content or initial conductivity than in HCP center) are consistent with a more gradual decrease in conductivity over time (in comparison to drier and more resistive locations such as in HCP-center).

Estimation of in situ unfrozen water content over time was performed using bulk electrical conductivity and temperature data and various petrophysical relationships and parameterizations (Figure 5). Unfrozen water content was estimated at two depths (0.25 and 3 m) under the LCP center. At 0.25 m depth in LCP center, unfrozen water content was calculated from bulk electrical conductivity and temperature using equations 1–3. The equations were parameterized with an initial solute concentration equal 0.4 g/L, and total water content and saturation equal to 0.6 and 1, respectively, based on soil sample analysis. Setting the a exponent equal to 0.5 suggests that at the lowest temperature (~-13°C), unfrozen water content may be as high as 5% and at -2°C, the unfrozen water content may be as high as 10% of the total volume of soil. In contrast, setting the a exponent to 1 suggests that the unfrozen water content may be only 2% at the lowest temperature, while at -2°C the unfrozen water content may be 4%. Using equations 1, 2, and 4 instead suggests even a smaller unfrozen water content of 3% at -2°C. The

largest unfrozen water content estimated using the a exponent equal to 0.5 is the most consistent with previous studies at the lab scale as well as point-scale indirect measurements collected at the field scale. These previous studies suggest that the unfrozen water content value of the highly organic soils in Barrow, AK, is about ~15% at -2°C [Romanovsky and Osterkamp, 2000], that winter organic soil has average value of 6% saturation [Hinzman et al., 1991; Liljedahl et al., 2011], and that clay soils with various total water contents had unfrozen water content values between 11% and 19% at -10°C [Suzuki, 2004; Karra et al., 2014]. The strong variability in soil properties, the complexity of the freezing process, and the technical limitations in measuring unfrozen water content and salinity during freezing partly explain the wide range of estimates.

We also explored the range of unfrozen water in regions of the permafrost that revealed very limited changes over time. At 3 m depth below the LCP center (Figure 5), unfrozen water content was calculated from bulk electrical conductivity and temperature and using equation 1–3 parameterized with an initial solute concentration equal 5 g/L, and total water content and saturation estimates equal 0.4 and 1, respectively, based on soil sample analyses at the NGEE-Arctic site [Dafflon et al., 2016]. Setting the a exponent equal to 0.5 suggests that at the highest temperature ($\sim -5^{\circ}\text{C}$), unfrozen water content may be as high as 19%. In contrast, setting the a exponent equal to 1 suggests that the unfrozen water content may be 10% at the highest temperature. Using equations 1, 2, and 4 implies even a smaller unfrozen water content of 8%. These estimations have high uncertainty due to limitations in data, models, and process understanding. Regardless, unfrozen water content at other locations at the site may be much higher than along the intensive monitoring transect, given that ERT electrical conductivity values along the monitoring transect are relatively low compared to other locations at the site (as revealed through comparison of Figures 2 and 10).

4.2 Dynamics in Thaw Layer and Vegetation During the Thaw-Growing Season

In this section, we explore the spatiotemporal interactions between thaw layer properties and vegetation dynamics during the thaw and growing seasons. Several figures are used to support this discussion. Figure 6 shows the comparison between measurements collected at various time intervals along the intensive monitoring transect. Measurements include bulk electrical conductivity extracted from the top 20 cm of ERT time lapse images (which likely represents some weighted averaged function of the 0–40 cm interval) and green chromatic coordinate values extracted from the time lapse images from the pole-mounted cameras, TDR data, and snow and thaw layer thickness measurements. Figure 7 shows the relationship between the bulk electrical conductivity of the ERT top 20 cm and the green chromatic coordinate from the

aboveground images over time, and Figure 8 shows the relationship when considering NDVI value instead of the green chromatic coordinate. Figure 9 shows the cross correlation between all the properties (most of them measured on 24 July 2014), as well as the link between soil and vegetation properties and the various polygon types. We use these figures to discuss codynamics within and across the thaw layer and vegetation compartments of the Barrow ecosystem.

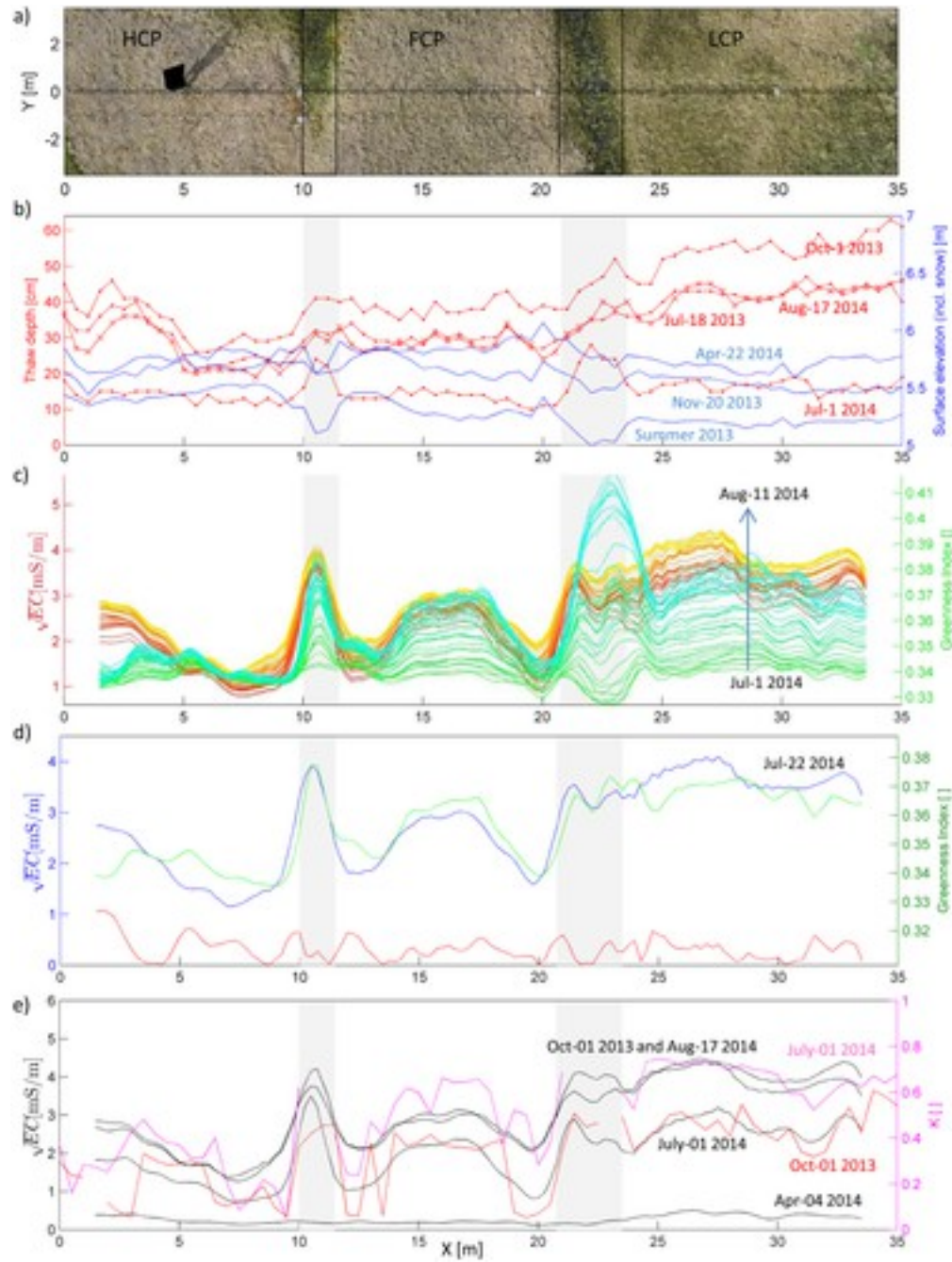


Figure 6
[Open in figure viewer](#)[PowerPoint](#)

(a) Aerial view of the transect monitored with ERT and pole-mounted cameras. (b) thaw depth, surface elevation and top of snow elevation measured at various times. (c) Top 20 cm soil electrical conductivity values estimated daily from 1 July (day 0) (red) to 11 August (day 40) (yellow) and green chromatic coordinate calculated for the same period (green to blue). (d) measured bulk electrical conductivity (blue) and measured green chromatic coordinate and inferred bulk electrical conductivity (green) using the linear relation obtained on 22 July (strongest correlation) (Figure 7b), and absolute difference between them (red). (e) bulk electrical conductivity (black) and relative dielectric permittivity (from TDR) in the top 10 cm (pink and red) collected at several times during the monitoring period.

Caption

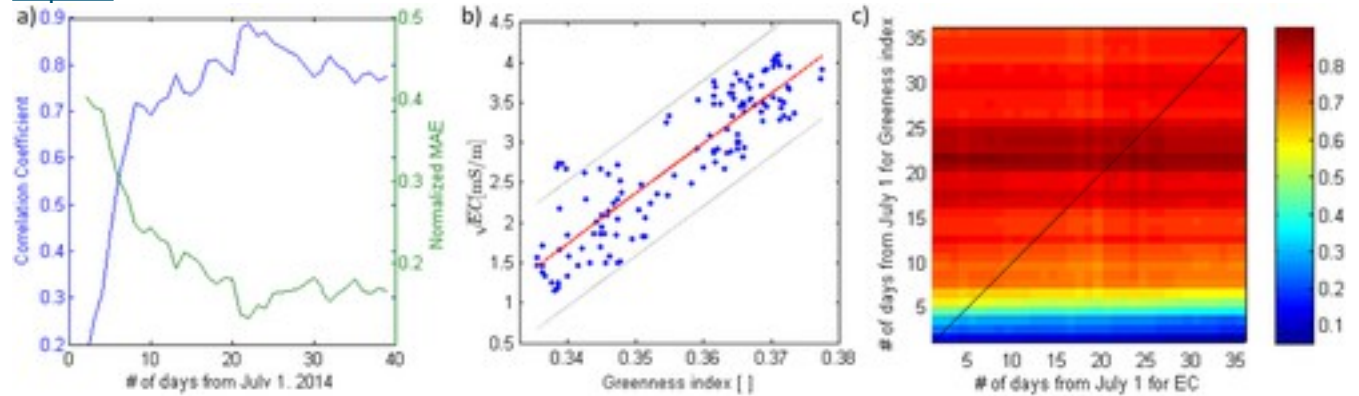


Figure 7

[Open in figure viewer](#) [PowerPoint](#)

(a) Correlation and normalized mean absolute error between soil bulk electrical conductivity (in the ERT top 20 cm) and green chromatic coordinate from 1 July (day 0) to 11 August (day 40) 2014. (b) Linear relationship between spatial distribution of green chromatic coordinate and bulk electrical conductivity on 22 July 2014, with grey lines indicating the relationship ± 2 times the standard deviation of the residual distribution ($r = 0.89$). (c) Cross correlation between electrical conductivity and green chromatic coordinate (black line indicate the 0 day time lag of one relatively to the other) showing that green chromatic coordinate values around 22 July (20 to 25 July) correlate best with electrical conductivity values at similar times and also at different times mainly because electrical conductivity values are more strongly autocorrelated over time than green chromatic coordinate.

Caption

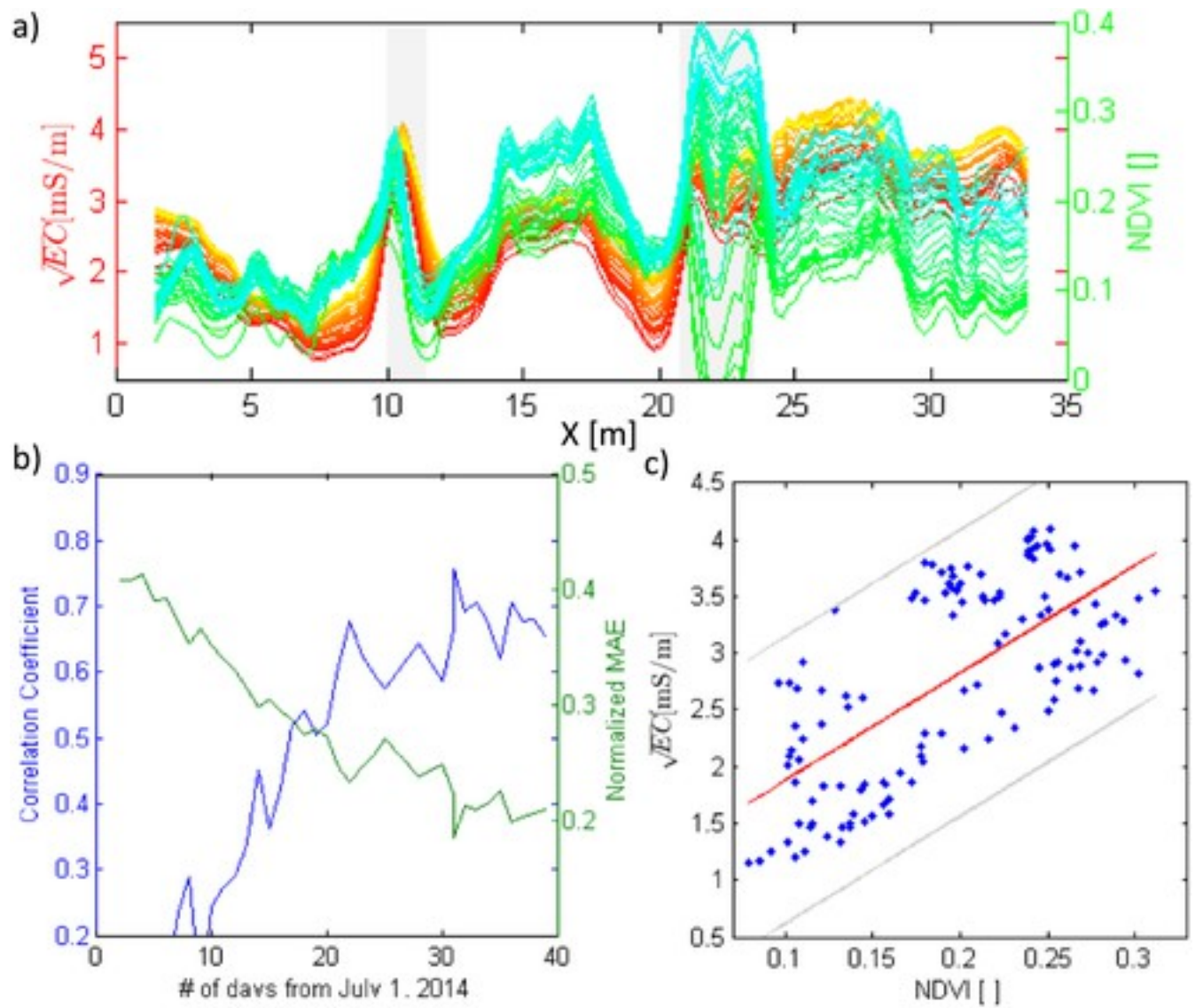


Figure 8

[Open in figure viewer](#) [PowerPoint](#)

(a) Soil bulk electrical conductivity values (in the ERT top 20 cm) inferred daily from 1 July (day 0) (red) to 11 August (day 40) (yellow) (same as Figure 5c) and NDVI calculated for the same period (green to blue). (b) Correlation and normalized mean absolute error between bulk electrical conductivity and NDVI from 1 July (day 0) to 11 August (day 40). (c) Linear relationship between NDVI and bulk electrical conductivity on 29 July with grey lines indicating the relationship ± 2 times the standard deviation of the residual distribution ($r = 0.72$).

[Caption](#)

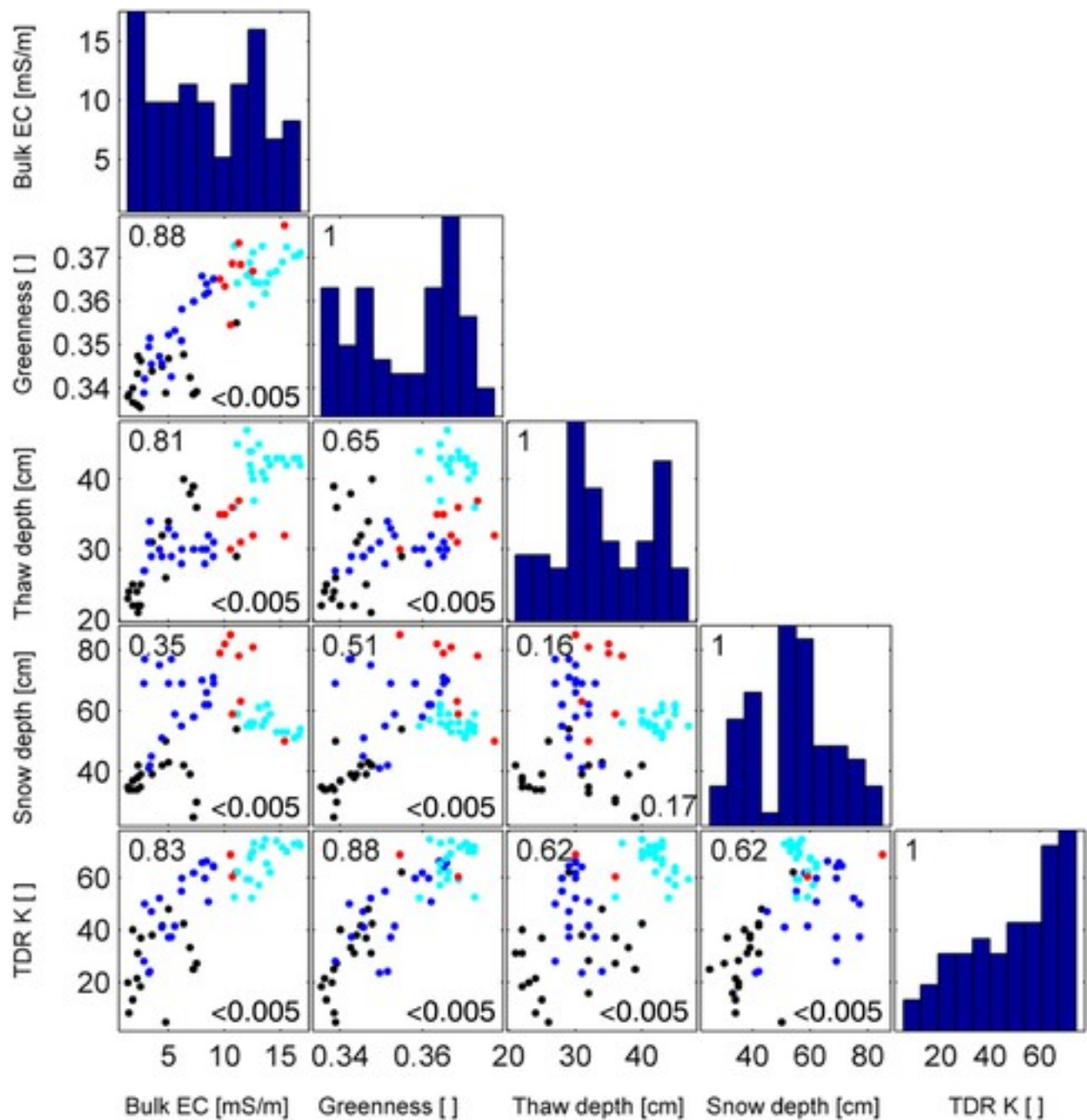


Figure 9

[Open in figure viewerPowerPoint](#)

Cross correlation between properties (points) and relative frequency distribution of properties (bars), including green chromatic coordinate, bulk electrical conductivity, and thaw depth (deeper thaw depth implying higher temperature at a specific depth) collected on 24 July 2014, TDR data collected on 1 July 2014, and snow thickness collected on 22 April 2014. Colors refer to HCP (black), FCP (blue), LCP (light blue), and troughs (red). The correlation coefficients and their statistical significance (p values) are shown in each cross-correlation plot on the top left and bottom right corners, respectively.

[Caption](#)

4.2.1 Water Content and Thaw Layer Codynamics

The thickness of the active layer is an important aspect of ecosystem functioning, as it corresponds directly to changes in soil temperature, which with moisture strongly influence biogeochemical processes [e.g., *Wainwright et al.*, [2015](#)]. Figure 6 shows that thaw layer thickness at the end of the growing season is as thin as 30 cm in the center of the HCP and up to 65 cm in the center of the LCP, exhibiting more than 100% variation along the intensive transect. During most of the growing season (except at the early beginning of growing season as shown in Figure 3), the maximum in thaw layer thickness is located at the center of the LCP, and the minimum is located at the center of the HCP. After the beginning of the growing season, the thickening rate of the thaw layer is faster at the LCP center than at the HCP center and remains larger during the remainder of the growing season. The LCP and the HCP can be considered end-members, while the active layer dynamics of the FCP during thaw and the growing season is intermediate between these two end-members. The time lapse ERT images emphasize the importance of spatial variations in active layer dynamics as a function of geomorphology.

Our data revealed a strong correlation between thaw layer thickness and water content proxies, such as bulk electrical conductivity extracted from the top 20 cm of ERT time lapse images, and dielectric permittivity of the top 10 cm of soil inferred from TDR measurements (Figure 8). As an example, the correlation coefficient between thaw layer thickness and shallow electrical conductivity measured on 24 July 2014 is 0.81, and the correlation between thaw layer thickness and dielectric permittivity is equal to 0.62. These significant correlations confirm that the thaw layer thickness is covarying with soil moisture and other soil properties and that its variability is well represented by shallow soil electrical conductivity. The correlations also suggest that soil temperature below the pure organic layer, which is a strong indicator of thaw layer thickness [*Jorgenson et al.*, [2010](#)], is expected to be correlated with soil electrical conductivity.

Comparing different techniques used to estimate water content variations highlights the control of the TDR and bulk electrical conductivity measurement support scale on the obtained value. Although TDR and electrical conductivity show very similar trends, TDR, because of its shallow and small volume of influence, tends to show wetter conditions at the beginning of the growing season than at the end, while ERT (which has a larger measurement support scale and may even be influenced by the underlying permafrost) shows the opposite trend (Figure 6e). While the depth integrated amount of water in the thaw layer at each location along the transect increased during the growing season due primarily to the thickening of the thaw layer, the top organic layer (top 7 to 15 cm) that influences the TDR response became dryer with time. Furthermore, while the correlation coefficient between TDR and electrical conductivity is significant ($r = 0.83$)

(Figure 9), it rarely increases. Measurements along many other transects at this site (not shown here) have demonstrated similar correlation coefficients (ranging between 0.65 and 0.85) between both parameters. A main reason is that ERT and TDR are sensitive to water content as well as other soil characteristics that they each weight differently. While they can both measure water content accurately once calibrated for soil (and when properties other than water content do not vary significantly over space), the Arctic tundra active layer typically reveals significant spatial variability of volumetric fraction of organic, mineral, and porosity. This partly explains the difference between and value of various measurement approaches and why soil moisture measurements in the Arctic need to be compared carefully. While TDR is physically more uniquely sensitive to water content variations than ERT, the ERT is likely a better integrator of the various controls on vegetation dynamics.

The influence of the natural year-to-year difference in meteorological conditions between 2013 and 2014 on the thaw layer thickness is also revealed in Figure 6a. For example, the thaw layer thickness observed in August 2014 is smaller than in August 2013 and is similar to the thickness observed during July 2013. This smaller thaw layer thickness also means lower soil and permafrost temperatures because of the shallower position of the 0°C isotherm. This 1 month shift in dynamics in soil and permafrost is also observable in the ERT data (Figure 2). While the relative spatial variability in resistivity does not change significantly from 1 year to the next, the time shift in resistivity is controlled by meteorological conditions, as shown in this case, where the air temperature in 2014 was generally colder than in the previous year. This difference in air temperature is reflected in the soil electrical conductivity values, which are similarly lower in August 2014 compared to August 2013.

4.2.2 Codynamics in Bulk Conductivity and Vegetation Greenness

The green chromatic coordinate and electrical conductivity values show similar trends along the monitoring transect (Figure 6c). Electrical conductivity values from 1 July to 11 August reveal significant yet consistent lateral and temporal variability. The green chromatic coordinate (estimated along the transect from the landscape images) transitions from a low value and minimal spatial variability on 1 July to higher values and greater spatial variability, revealing a spatial trend similar to the electrical conductivity. The green chromatic coordinate shows much lower autocorrelation between different times in the season compared to electrical conductivity. The autocorrelation is degraded by the very strong temporal variations associated with troughs, where standing water is replaced by dense vegetation (10–12 m and 21–24 m) and by temporal variations in the centers of FCP and LCP, where grass grows on a relatively muddy ground at the beginning of the growing season.

While at the beginning of the growing season the green chromatic coordinate does not correlate with electrical conductivity, the correlation coefficient rapidly increases during the growing season starting 1 July and reaches a peak in correlation ($r = 0.89$) on 22 July (Figure 7a). The best fitting linear relationship between the spatial distribution of electrical conductivity and green chromatic coordinate is shown for 22 July (Figure 7b). When the trough regions are omitted (not shown), the correlation coefficient between the green chromatic coordinate and electrical conductivity rises to 0.91 on the same date. Further, while the highest correlation between green chromatic coordinate and electrical conductivity is observed on 22 July, the green chromatic coordinate at that time is highly correlated with electrical conductivity almost every day from 1 July to 11 August, with correlation always higher than 0.8 (Figure 7c).

While the electrical conductivity does change over that time period, its spatial variability along the transect is highly autocorrelated over time. This means that the soil water content spatial distribution at any time can potentially be used to predict the spatial variability of green chromatic coordinate, or, more importantly, the green chromatic coordinate spatial distribution at the peak of the growing season can be used to predict the spatial variability of water content. Inferring absolute values requires a few ground-based water content measurements at intensive sites. To test this hypothesis, the green chromatic coordinate values obtained on 22 July are used to predict electrical conductivity using the inferred linear relationship (Figure 6d). The residual between measured and predicted electrical conductivity shows that the correlation between the green chromatic coordinate and electrical conductivity is smallest for the first 3 m along the transect. This interval shows very specific behavior with deep active layer and high electrical conductivity, but a very small green chromatic coordinate value. This behavior is likely due to the presence of a small nonsorted circle at this location implying higher mineral fraction compared to other locations along the transect. Such residual indicates that soil characteristics other than water content still have some influence on the vegetation distribution, and that the inferred empirical relationships have limitation.

The correlation between the NDVI and the electrical conductivity (Figure 8) shows a similar trend as for the green chromatic coordinate and electrical conductivity over time, with a maximum correlation coefficient fluctuating between about 0.65 and 0.72 during the period 22 to 29 July. The green chromatic coordinate revealed spatial and temporal landscape variability, with similar trends as NDVI, but the estimates were less sensitive to changes in light and weather conditions. NIR may be preferable for investigating phenology when using narrow spectral bands, while the use of a standard camera implies nonnarrow and slightly overlapping bands. Another difficulty in using a standard camera modified for NIR sensitivity is its tendency to have

a strong correlation between the various channels that limit the quality of any calibration [Nijland *et al.*, 2014]. Ongoing development of relatively simple, multispectral cameras, with relatively narrow bands, offers a promising approach to improve estimates of vegetation indices using low-altitude, aerial imaging.

4.2.3 Soil and Vegetation Property Codynamics

While the importance of interactions between thaw layer and vegetation compartments of ecosystems are recognized, the dense and autonomous measurements provided by our sensing system has allowed the first “visualization” of the spatiotemporal interactions between the compartments. Figure 7 illustrates the codynamics between green chromatic coordinate (a proxy for vegetation vigor) and electrical conductivity (a proxy for soil moisture), particularly revealing that the peak of the correlation ($r = 0.89$) is at the peak of the growing season. Figure 9 shows that thaw layer thickness, a direct indicator of the soil temperature and root available unfrozen soil and soil water content, is also strongly correlated with both electrical conductivity and green chromatic coordinate. Also, the spatial variability in soil electrical conductivity and thaw layer thickness well before the peak of the growing season are strong indicators of the spatial distribution of the green chromatic coordinate at the peak of the growing season (Figure 6). This finding emphasizes the influence of the spatial distribution of soil characteristics on the vegetation growth. Because vegetation growth is likely controlled by various parameters including thaw thickness, soil structure, soil water content, and soil temperature, the bulk electrical conductivity effectively serves as a diagnostic indicator of soil attributes important for vegetation dynamics.

In addition to the significant temporal relationships observed between various properties, the relationships also vary as a function of geomorphology (Figure 9). For example, Figure 9 shows that the distribution of and correlation between various properties are strongly clustered as a function of HCP, FCP, and LCP polygon type as well as by polygon feature (e.g., trough). This finding is consistent with *Wainwright et al.* [2015], who suggested that polygon type greatly influences aboveground and belowground property variability in Arctic tundra, and that probabilistic distribution of polygon type can provide useful information about critical property suites over landscape scales. Our results show that the type of polygon does not only control distinct property distributions at the peak of the growing season, but that polygon type also controls distinct temporal behavior. For example, in Figure 6 the change in green chromatic coordinate, thaw layer thickness, and electrical conductivity during the growing season is largest in the LCP and smallest in HCP. This is also obvious when looking at Figure 3, which shows that

HCP tends to reach a much colder temperature and lower water content than LCP during the winter.

4.2.4 Scaling Up Findings From Intensive Monitoring Transect

To evaluate the robustness of the developed relationships between green chromatic coordinate around the peak of the growing season and the electrical conductivity from ERT at any time of the growing season, we compared the green chromatic coordinate extracted from the landscape mosaic obtained on 12 July 2013 over the regional transect (Figure 1b) and the collocated bulk electrical conductivity averaged over the top 20 cm of the ERT data along the 470 m long profile acquired in September 2012 (Figure 10). The resulting correlation between the green chromatic coordinate and the bulk conductivity of the top 20 cm of the long ERT transect is 0.75 (or 0.79 if the intervals where ponds with surface water are present are removed). While acquired at a different time period, this high correlation is consistent with the finding along the intensive monitoring transect and confirms the strong growing season relationship between belowground (soil electrical conductivity) and aboveground (green chromatic coordinate) measurements. If this relationship can be documented or developed at other sites, it opens the door for using easily acquired optical data (ideally with topography information) to estimate growing season soil properties, or vice versa.

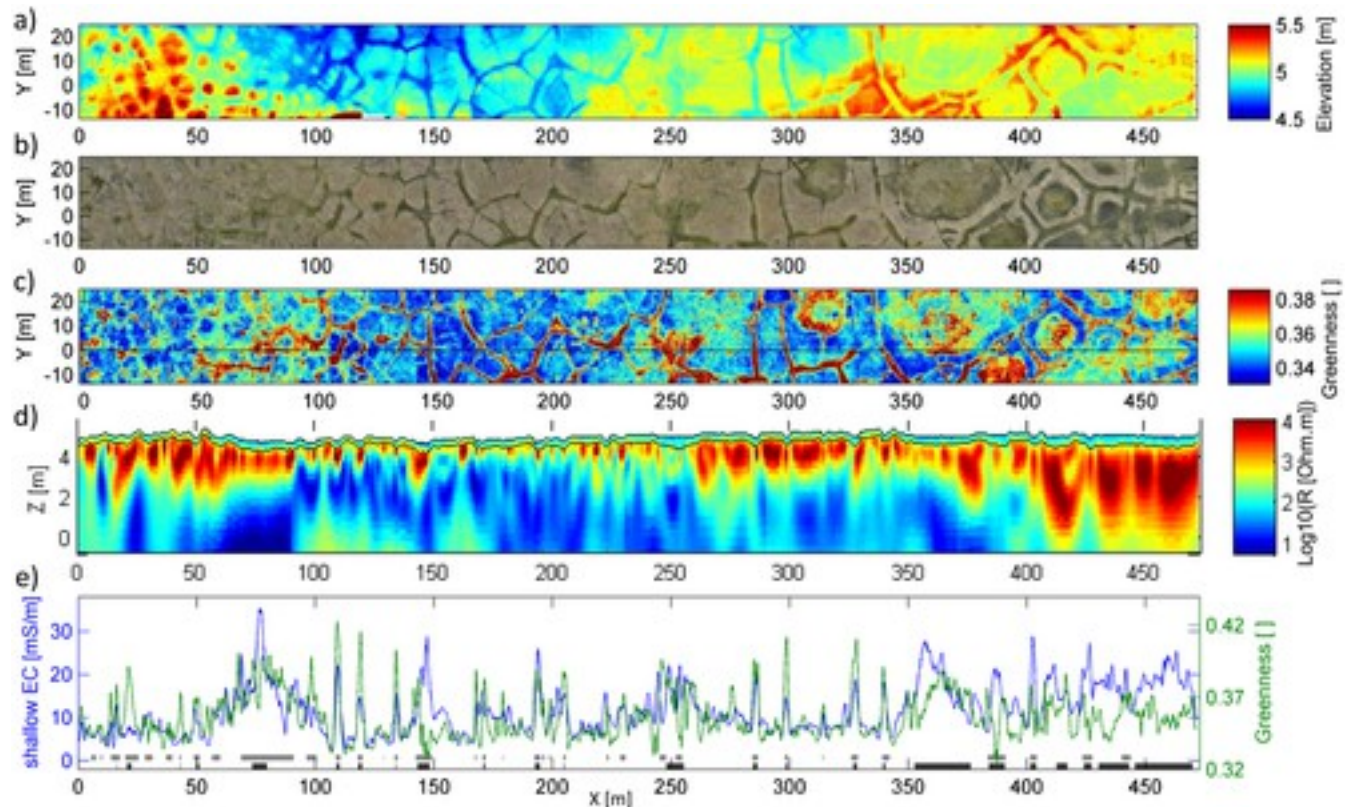


Figure 10

[Open in figure viewer](#)[PowerPoint](#)

(a) Surface elevation along a 450×40 m corridor (location shown in Figure 1), (b) corresponding RGB mosaics obtained on 12 July 2013 and (c) inferred green chromatic coordinate, (d) ERT acquired in September 2012 along the transect shown with the black line in Figure 10c, and (e) green chromatic coordinate (extracted from Figure 10c) along the ERT profile) and bulk electrical conductivity of the top 20 cm in ERT (extracted from Figure 10d). The black and grey intervals in Figure 10e indicate location of surface water and troughs, respectively.

[Caption](#)

5 Conclusions

Improving predictive understanding of Arctic ecosystem dynamics and evolution requires advances in quantifying soil hydrological and physical properties of the active layer and permafrost, their interactions with vegetation properties, and the influence of geomorphology on both aboveground and belowground properties. In this study, we investigated subsurface and surface dynamics and their interactions along a 35 m long transect in polygonal-shaped tundra in Barrow, AK, by developing and applying a novel monitoring approach. The approach included joint data monitoring and analysis from autonomous ERT (to sense soil and permafrost dynamics) and pole-mounted cameras (to sense land surface and vegetation dynamics), together with depth profiles of soil temperature and occasional measurements of thaw layer thickness, snow layer thickness, and TDR measurements.

Results of this study indicate significant codynamics between thaw layer thickness, soil properties, and vegetation growth in this Arctic environment. The soil electrical conductivity from ERT is strongly correlated with thaw layer thickness, which is indicative of the soil temperature and influences the total amount of unfrozen soil and water available for roots. The correlation between green chromatic coordinate and soil electrical conductivity increases during the growing season. The correlation increases to a maximum correlation coefficient of 0.89 at peak of the growing season, documenting the significant interactions between aboveground and belowground process. While the most significant correlations are observed between green chromatic coordinate, soil electrical conductivity, and thaw layer thickness, our study revealed that TDR and snow thickness are also covariates. The distribution of soil properties and the spatiotemporal expression of all soil and vegetation dynamics are also shown to vary with polygon type and the polygon-controlled microtopography. Our results suggest the possibility of using greenness maps of Arctic tundra obtained using UAS-, aircraft-, or satellite-based platform, to infer soil properties during the growing season. Successful application of the

aboveground and belowground approach to a nearby 470 m long ERT transect demonstrates the potential for scale-up.

This study also led to some new insights about the local spatial variability in freeze-thaw perturbations and its influence on permafrost, soil and surface properties. Results show that the freeze-thaw process in the active layer can vary significantly based on polygon-specific soil and surface properties. Indeed, the largest conductivity values are observed below the LCP center (due primarily to the relatively higher water content) and the conductivity values decrease relatively slowly over time in comparison to drier and more resistive locations (such as below the HCP center). Due to the complex coupling between fluid salinity, total water content, and soil constituents fractions influencing the soil freeze-thaw behavior, estimation of unfrozen water content using ERT is challenging but can be reasonably performed using petrophysical relationships and benefit from supporting measurements. This study also revealed significant seasonal dynamics in the permafrost, leading to significant variations in unfrozen water content and salinity. Unfrozen water content at 3 m depth is the highest around December and can potentially reach 10 to 20% volume fraction along the intensive transect. These values can potentially be even larger at other locations at the Ngee site given the spatial variability in soil electrical conductivity observed at larger scale at the site. Investigating the active layer freeze-thaw behavior as well as transients in the high solute concentration permafrost are important given their joint influence on water content, water fluxes, microbial activity, and permafrost thawing occurring at temperatures below 0°C. These processes in turn contribute to a number of important societal issues, including greenhouse gas release, rate of coastal erosion and permafrost degradation, particularly as related to infrastructure stability in coastal regions susceptible to saline intrusions. Investigation of freeze-thaw dynamics and coupling between permafrost-soil-vegetation processes using hydro-thermal-geophysical inverse modeling is ongoing.

To our knowledge, this is the first study to develop and test an autonomous approach to simultaneously monitor aboveground and belowground properties and to use obtained data to explore interactions across permafrost, soil, land surface, and vegetation compartments of a dynamic ecosystem. It yielded many scientific insights that would have been difficult to obtain using conventional (point-based) monitoring approaches. While developed and successfully tested in an Arctic ecosystem, the new aboveground and belowground coincident monitoring approach can be applied to larger regions and be used for exploring complex dynamics in a variety of ecosystems.

Acknowledgments

The Next-Generation Ecosystem Experiments (NGEE-Arctic) project is supported by the Office of Biological and Environmental Research in the DOE Office of Science. This NGEE-Arctic research is supported through contract number DE-AC02-05CH11231 to Lawrence Berkeley National Laboratory. Logistical support in Barrow was provided by UMIAQ, LLC. The authors thank Bill Cable (University of Alaska at Fairbanks) for helping to install thermistors and providing soil temperature data, Stan Wullschleger (NGEE-Arctic PI, ORNL) for support and field assistance, A. Kemna (University of Bonn) for providing 2-D complex resistivity imaging codes, and C. Tweedie and S. Vargas (University of Texas at El Paso) for providing advice about kite-based aerial imaging. Data sets are available upon request by contacting the corresponding author (Baptiste Dafflon, bdafflon@lbl.gov) and from the NGEE-Arctic data repository [Dafflon *et al.*, 2017] (<https://doi.org/10.5440/1355348>).